# Aluminium Oxide Thin-Film based *in vitro* Cell-Substrate Sensing Device for Monitoring Proliferation of Myoblast Cells

Uvanesh Kasiviswanathan, Chelladurai Karthikeyan Balavigneswaran, Chandan Kumar, *Member, IEEE,* Suruchi Poddar, Satyabrata Jit, *Senior Member, IEEE*, Neeraj Sharma*, and Sanjeev Kumar Mahto*

***Abstract*— We demonstrate cell-substrate interaction on aluminium oxide thin-film in metal-insulator-metal structure followed by the change in dielectric characteristics of $Al_2O_3$ as a function of progression of cellular growth. The theoretical calculation of the fabricated biosensor reveals that the changes in the intrinsic elemental parameters are mainly attributed to the cell-induced behavioural changes.**

***Index Terms*—Aluminium oxide, Cell interaction, MIM structure, Myoblast Cells, Mathematical modelling.**

This work was supported in part by the Biotechnology Industry Research Assistance Council (BIRAC), an initiative under Department of Biotechnology (DBT), Ministry of Human Resource and Development (MHRD), Gov. of India for the grant and the SITARE-BIRAC-GYTI award (*Project id: 13246, 2019*) under student's innovations for translation & advancement of research explorations (SITARE) scheme

Uvanesh Kasiviswanathan, Chelladurai Karthikeyan Balavigneswaran, Suruchi Poddar, Neeraj Sharma and Sanjeev Kumar Mahto are with the School of Biomedical Engineering, Indian Institute of Technology (Banaras Hindu University), Varanasi, U.P. 221005 India (email: uvaneshkasiviswanathan@gmail.com; neeraj.bme@iitbhu.ac.in; skmahto.bme@iitbhu.ac.in).

Chandan Kumar and Satyabrata Jt are with the Department of Electronics Engineering, Indian Institute of Technology (Banaras Hindu University), Varanasi, U.P. 221005 India.

*These authors are corresponding authors.

## I. Introduction

CELLS are the basic building blocks of all organism, which govern all functional aspects of the complex heterogeneous biological system. Any abnormality in a single cell affects the entire characteristic behaviour of tissues, organs, and even organisms [1]. For example, Cancer is a complex genetic disease caused by an abnormal alteration (mutations) in DNA sequences that lead to disregulation of normal cellular processes, thereby driving tumor growth [2], [3]. Therefore, it is necessary to understand the complex biological system at their cellular level to develop new drug targets and treat any complex diseases. Cell-based biosensors (CBB) are extensively used to determine phenotypic changes of cells and found their potential application to study cell growth, apoptosis, wound healing, *in vitro* toxicological studies, drug screening, etc. [4]–[6]. A CBB is an analytical device that uses living cells as an analyte (i.e., transducer or the detecting or sensing element) for monitoring *in vitro* changes in cell physiology electronically [7]. The cell-material interaction is influenced by the substrate's physicochemical and structural properties that control the progression of cellular function [8]–[10]. In particular, the adherent cell establishes an active communication with the extracellular microenvironment *via* the membrane proteins, i.e., integrins, a cell membrane-bound receptor, which help cells to adhere on the substrate [11], [12]. Due to progression of cell cycle, it forms a monolayer of cells on the surface of a substrate [13]–[16].

The commonly used dyes to sense the cell proliferation include as fluorescein diacetate (FDA), calcein AM, acrydin orange, 4′,6-diamidino-2-phenylindole (DAPI) and indirectly by estimating tetrazolium salts in XTT and MTT assays [17]. However, the dynamic or real time activity of the cells cannot be quanitified with such conventional methods. Recently, cell trackers have been used to trace the dynamic behaviour of the cells, which pass through the cell membranes into cells and transformed into a cell-impermeant fluorescent product [18]. Further, nanoparticle-based cell trackers such as carbon quantum dots [19], graphene NPs [20] have also been studied. The traditional methods of monitoring cellular transformation mentioned above furnish us with either qualitative or semi-quantitative data apart from the requirement of its labour

intensive protocols and expensive equipment. Moreover, these assays greatly disturb the normal physiological state of the cells resulting in their destruction [21]. Therefore, for precise monitoring of the cellular behaviours in response to external stimuli, a real-time, non-invasive and label-free method is desirable. Since 1900s, impedance measurements of biological systems is used as a non-destructive label-free method to measure the electrical properties of cells [22]–[24].

Various CBBs have already been reported [25]–[32]. In a typical work, Sticker *et al*. [4] reported an improvement in the reliability of impedimetric sensors for cell analysis using electrically insulated zirconium dioxide ($ZrO_2$) nanolayer coated gold (Au) interdigitated electrode (IDE). They also revealed that this sort of arrangement provided an even distribution of current across the sensing area towards the analyte (i.e., adherent cells). Further, Schmiedinger *et al*. reported the fabrication of aluminium and titanium IDE's and investigated its performance by monitoring epithelial barrier functionality of two adherent tissue models *via* ECIS method [33]. While, Zhang *et al*. reported monitoring of cellular adhesion and spreading processes through plasmonic Al nanopyramid array sensor [34] and nanoplasmonics-enhanced label-free imaging of endothelial cell monolayer integrity by Banville *et al.* [35]. Recently, we have reported a detailed investigation to determine the dynamic behaviour of adherent mammalian cells using a metal-semiconductor-metal (MSM) device. The electrical change in the semiconducting ZnO thin-film in MSM device was observed mainly due to the progression of cellular functions [36]. Therefore, the electrical properties of the thin-film are important to study the progression of functional aspects of the cells.

An electrically insulating aluminium oxide ($Al_2O_3$) has shown attractive features for biosensing applications including its biocompatibility [37], [38]. It is a metastable dielectric material having wide bandgap of about ~6.7 eV at room temperature ( ~ 25°C) and variable lattice structures with strong Al-O bonds [39]. Metastable polymorph structure of $Al_2O_3$ results in the various phase transition state at different temperatures such as γ, η, δ, θ and χ. However, thermodynamically α-$Al_2O_3$ (corundum) transition phase is found more stable than all the other phases [40]. When $Al_2O_3$ is annealed at a temperature below 400°C, it forms the amorphous structure with the different types of arrangements, such as short-range order and long-range disorder. Additionally, α-$Al_2O_3$ is reported to show high mechanical strength, hardness, thermal conductivity, corrosion, and abrasion resistance. Also, the α-$Al_2O_3$ has a high dielectric constant at least twice that of silicon dioxide ($SiO_2$). Hence it is used widely as electrical insulators, tunneling barriers, radiation-resistant materials, optical material in electronic and optoelectronic applications. It is also considered to be an alternative dielectric material to silicon-based devices [41]. $Al_2O_3$ based materials have been reported to be biocompatible and the cytotoxicity of the material is found to be significantly lesser than ZnO, $TiO_2$, $SiO_2$, $FeCl_3$, and $Co_3O_4$ [42], [43]. In addition, the transparency of the $Al_2O_3$ thin film of the group III-VI is advantageous in terms of imaging of the adherent mammalian cells.

In the present work, we have integrated the electrically insulating and transparent $Al_2O_3$ thin films to study the dynamic behaviour of cells. In order to support the cell adhesion, the $Al_2O_3$ thin-film was functionalized with gelatin. We have used mouse myoblast (C2C12 cells) as the model cell to examine the efficacy of our device. We have made an attempt to obtain a large sensing area (using $Al_2O_3$ thin film) for the adherent cells to facilitate the performance of its basic functionality in order to improve the existing *in vitro* cell impedance sensor. It is found that the electrical characteristic properties of the $Al_2O_3$ thin film are influenced due to the progression of cellular functional behaviour. Thus, analyzing the change in electrical characteristic properties of the $Al_2O_3$ thin film can divulge the current state of cellular function. Further, this sort of biosensor eliminates electrode fouling, bubble formation, etc., which generally occurs due to electrolysis and redox reactions between the cell culture medium and the electrode. To the best of our knowledge, $Al_2O_3$ thin film nanomaterial-based CBBs involving simplest procedures and non-sophisticated setup to determine functional and behavioural information of the adherent cell *in vitro* has not yet been reported.

## II. Materials and Methods

### A. Materials Used

Mouse Myoblast cell line (C2C12) was procured from NCCS, Pune, India. Dulbecco's Modified Eagle Medium (DMEM) high glucose, fetal bovine serum (FBS), penicillin-streptomycin (100 µg/mL penicillin and streptomycin), and gelatin type B (cell culture tested) were purchased from HiMedia India. Phosphate buffered saline (PBS, 10X) and ultrapure $Al_2O_3$ powder (99.99%) were bought from Sigma (Merck) India. High-temperature Teflon adhesive tape and single-side indium tin oxide (ITO) coated glass substrate (7×7 inch, ITO thickness = 150 nm) were procured from Macwin India Pvt Ltd, India.

### B. Biosensor fabrication

ITO coated glass substrate of 25 × 15 $mm^2$ was covered using Teflon tape and patterned to get an electrode dimension of 12 × 5 $mm^2$ at each side with a gap of 1 ± 0.2 mm (at centre) (**Fig. 1(a)**). The uncovered ITO regions were etched-out to get a co-planar electrode system, as shown in **Fig. 1(b)** using 9 M hydrochloric acid (HCl, 37%, Merck India) [36], [44]. Then, the patterned ITO coated glass substrates were thoroughly cleaned using standard wet chemical cleaning procedures. Contemporarily, ultrapure $Al_2O_3$ powder (99.99%) was mixed with a polymeric binder (polyvinyl alcohol, PVA) and pressed into a pellet. The pellet was heated for 3 h at 1200°C in the ambient air atmosphere to decompose the binder. Then, the heated $Al_2O_3$ pellet was used as the source material in the electron beam evaporation (EBE) unit (HINDVAC, Bangalore, India; Model No. FL400 SMART COAT 3.0 A). The $Al_2O_3$ pellets were vaporized on the cleaned patterned substrates at a deposition rate of ~5.00 Å/s to get a film of thickness ~100 nm in the EBE unit [45], [46]. The shadow masking technique is used to deposit the $Al_2O_3$ in the desired shape and size, as shown in **Fig. 1(c)**. The deposition rate and thickness of the film were monitored using the in-built digital thickness monitoring module (SQM-160, INFICON). Later, the obtained $Al_2O_3$ coated patterned ITO samples were annealed at 400°C in the inert (argon gas) atmosphere with about ~30 sccm argon gas

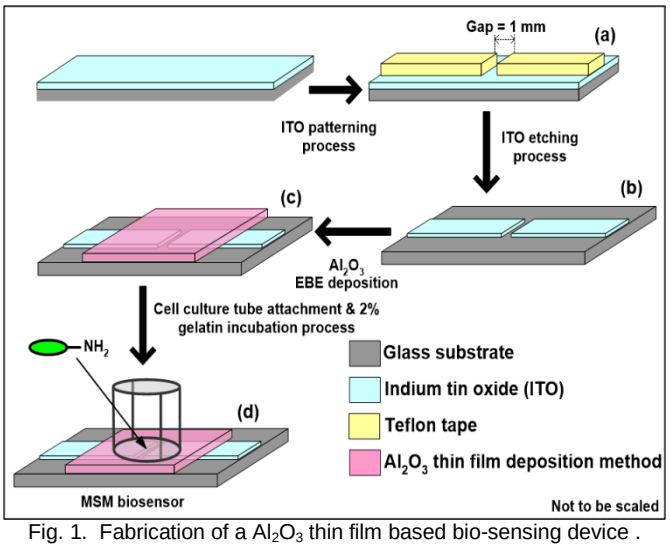


Fig. 1. Fabrication of a $Al_2O_3$ thin film based bio-sensing device .

flow for 1.5 h in the muffle furnace to obtain a crystallized $Al_2O_3$ thin film [47], [48]. A custom-designed polypropylene well was attached to the top of the substrates coated with $Al_2O_3$ thin film for maintaining the regime of the culture medium. The customized-well was sealed using polydimethylsiloxane (PDMS) (Dow Corning, Sylgard 184) to avoid the leakage of the culture medium [36]. Now onwards, we have mentioned this cell culturing device as the fabricated device (MSM biosensor), as shown in **Fig. 1(d)**.

### C. Cell culture procedure

Mouse myoblast C2C12 cells were maintained in a 5% $CO_2$ incubator (Galaxy 170S, Eppendorf) at 37º C with DMEM high glucose medium containing 10% FBS and 1% penicillin-streptomycin. The 2% gelatin coated on the fabricated device was used to culture the mammalian cells. The sub-cultured cells were grown inside the cell culture chamber attached to devices. The cell density of 4,000 cells/well was used for all the analyses performed. The cell culture medium was changed before every observation. The studies were done in triplicate (n= 3) and their average results were plotted.

## III. Results and Discussion

The outer environment of the cell is comparatively positive than the inner side of the cell. The potential difference across the cell membrane is maintained due to the various physiological processes, which govern the basic functionality of the biological cell. The C2C12 cells got adhered to the surface of gelatin coated $Al_2O_3$ thin film because of the cell-adhering moieties present in gelatin [49]. The adherence of cells on the substrate changed the characteristic electrical properties of the fabricated device, which could be attributed to the reduction in the free-flow of current across the active sensing area available. Furthermore, the electrical properties of the biological cells were reported to vary as a function of frequency. Researchers reported the current flow in and outside of the cell with respect to the frequency. In brief, the ions diffuse across the membrane at a lower frequency (< 1 kHz). Hence it is termed as 'α' dispersion. While, at mid frequency (1 kHz – 100 kHz), the current flow across the membrane is limited due to a Maxwell-Wagner phenomenon and it is referred as 'β' dispersion. On the other hand, at higher frequency (>100 kHz), the polarization of the water molecules present in that biological medium resulted in more current flow in the intracellular region than of the extracellular region of the biological cells, and it is termed as the 'γ' dispersion [1], [50].

Considering the electrical properties of the biological cells, we seeded 4000 cells/well on the fabricated device to study the effect of cellular functions and their behaviour. The change in the electrical properties was determined in terms of change in resistance/capacitance or impedance. The morphology of the grown cells was also observed over the time period of 72 h. Similarly, to analyse the frequency dominated changes – capacitance, the magnitude of impedance and phase of impedance *vs.* frequency plot were recorded and correlated with the microscopic images. From **Fig. 2(a)** (i.e., after 8 h), it was observed that the cells became flat, which implied that the cells started to grow on the underlying surface as it adapted to that micro-environmental condition. The growth of myoblasts over different time points showed a significant change in the

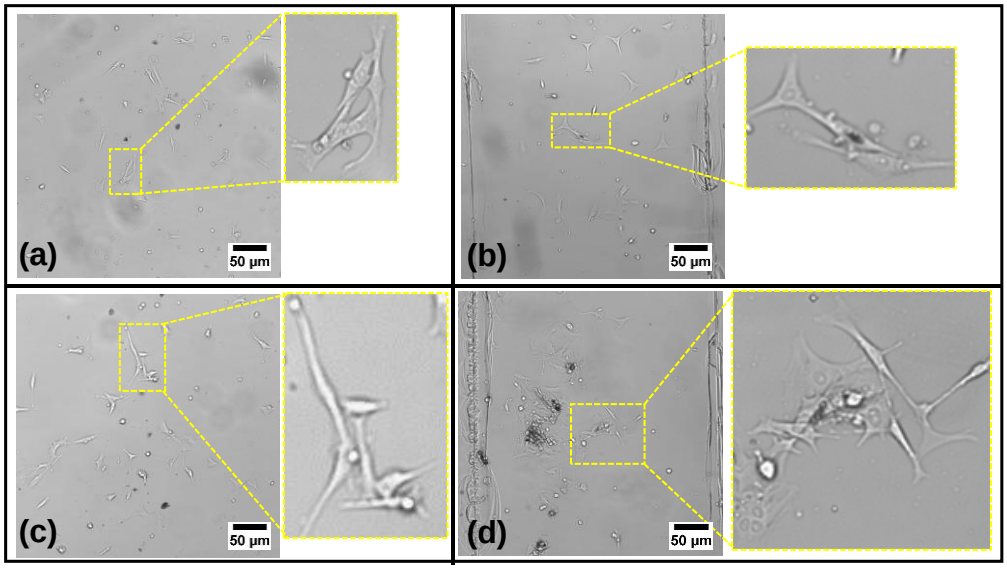


Fig. 2. Morphology of C2C12 cells at various time intervals: (a) 8 h, (b) 24 h, (c) 48 h, and (d) 72 h; Scale bar: 50 µm

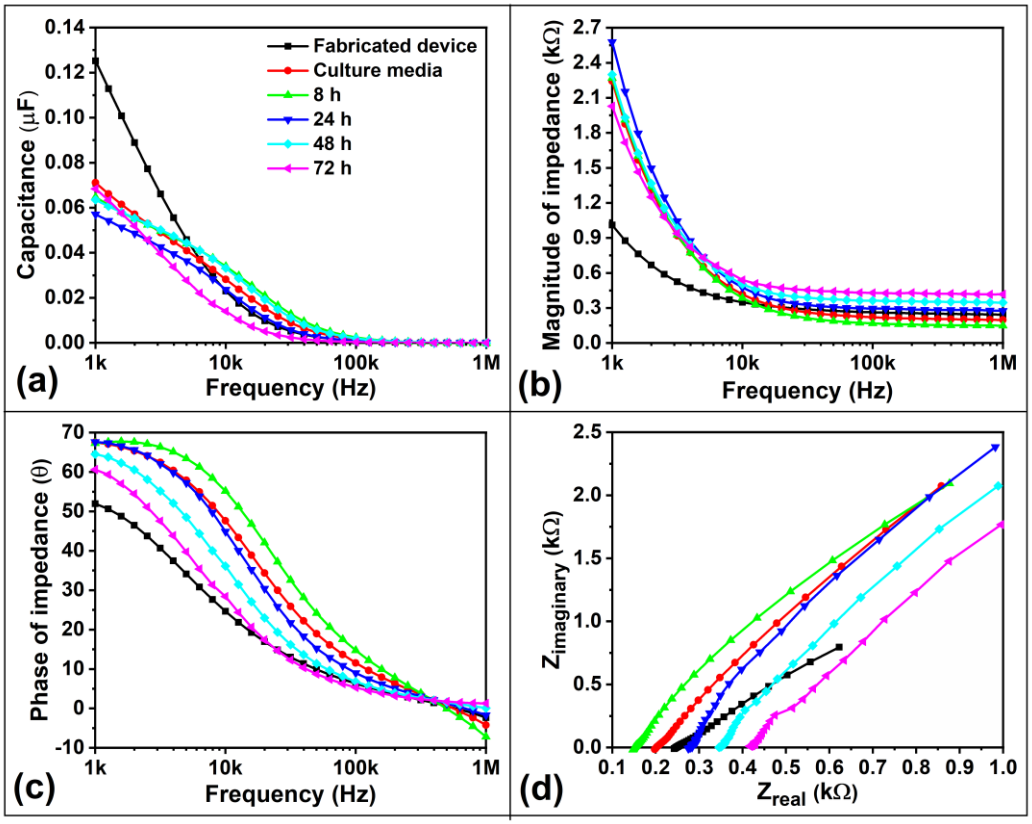


Fig. 3. Changes in the characteristic electrical properties of the $Al_2O_3$ thin film (a) capacitance *vs.* frequency plot, (b) magnitude of impedance plot, (c) phase of impedance plot, and (d) Cole-Cole (Nyquist) plot.

morphology, as observed in **Fig. 2(a-d)**. Moreover, the electrical characterisation results revealed that the capacitance values got decreased with an increase in the magnitude of impedance values and vice-versa, with the progression of cellular function, as shown in **Fig. 3(a)** and **3(b)**. Likewise, the phase angle is generally used to determine the degree of functionality of the cell membrane. i.e., when 'leaks' occur in the cell-membrane, the ability to maintain voltage decreases, so the phase angle decreases. Simultaneously, the cellular differentiation process decreases cell membrane resistance due to changes in the morphology of cells and increased intracellular space. A decrease in cell membrane resistance leads to increased cell membrane capacitance (increased cell membrane on the electrode's surface), which directly reduces the extracellular matrix resistance. Hence, change in the phase of impedance was directly correlated with change in the morphology of the cells [51], as shown in **Fig. 3(c)**.

The phasor diagram of complex impedance provides information about the level of energy dissipation of the system where, the real axis ($Z_{real}$) reflects the active resistance and the imaginary axis ($Z_{imaginary}$) reflects electrical capacitance and inductance of the system. Any shift in the magnitude is observed due to a change in resistivity and any shift in the angle is due to a change in phase of the system [44], [52]. The significant shift in the Cole-Cole (Nyquist) plot (**Fig. 3(d)**), was due to the progression of cellular functional behaviour on the surface of the substrate. Also, the increment in the impedance values was observed through the performance of the experiments, most likely due to the progression of cellular functional behaviour on the surface of the fabricated devices, which perhaps induced some capacitive effect on the surface of the thin-film device due to change in morphology as well as due to the cell-cell communication/interaction.

The magnitude of impedance data was used to fit the

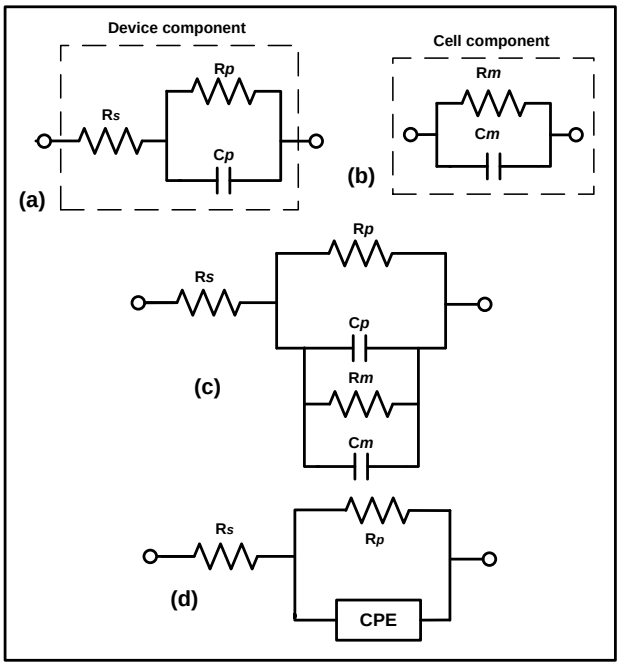


Fig. 4. Equivalent electrical circuit model (a) fabricated device component, (b) cell component, (c) fabricated device with cell component, and (d) cell-device.

TABLE 1. CALCULATED EEC MODEL PARAMETERS.

| Model Parameters | Fabricated device ($ITO/Al_2O_3/ITO$) | Culture medium on the fabricated device | cell-fabricated device | | | |
|---|---|---|---|---|---|---|
| | | | 8 h | 24 h | 48 h | 72 h |
| **n** | -- | 0.832 | 0.824 | 0.859 | 0.843 | 0.821 |
| **$Q_p$ (F)** | ($C_p$) $12.98 \times 10^6$ | $31.39 \times 10^6$ | $33.03 \times 10^6$ | $21.70 \times 10^6$ | $28.41 \times 10^6$ | $40.57 \times 10^6$ |
| **$R_p$ (Ω)** | 928.12 | $7.60 \times 10^5$ | $6.80 \times 10^5$ | $5.07 \times 10^5$ | $4.23 \times 10^5$ | $2.75\times 10^5$ |
| **$R_s$ (Ω)** | 271.02 | 200.73 | 136.36 | 269.54 | 338.37 | 407.43 |
| **$R^2$** | 0.992 | 0.999 | 0.999 | 0.999 | 0.999 | 0.999 |

equivalent electrical model to calculate the theoretical relationship between the surface-electrolyte-cell interface in the presence of biological cells [53]. **Fig. 4** shows the equivalent electrical model used in our study and **Table 1** shows the corresponding model parameters of the equivalent electrical model used. The equivalent electrical model was separated into device component and cell component to represent fabricated device containing biological cells. The fabricated device was depicted by RC circuit having a resistor (R*s*) in series with a resistor (R*p*) and capacitor (C*p*) in parallel, as in **Fig. 4(a).** As the cell membrane (C) acts as an insulator, it was represented with resistance (R*m*) and capacitance (C*m*). We considered the cell component with a resistor (R*m*) and capacitor (C*m*) in parallel combination, as shown in **Fig. 4(b).**

It has been reported that the current flows from the ITO electrode to the interfacing region upon excitation, wherein the transfer of electrons occurs [4]. The interfacing region in our device was $Al_2O_3$ thin film and the cell culture medium containing myoblast cells. However, the capacitance developed by the biological cells is anticipated to be more than the device capacitance. Hence, we replaced the device's capacitor (C*p*) with the cell component to represent the charged double-layer across the fabricated cell-device (surface-(electrolyte-cell interface)), as represented in **Fig. 4(c)** [23], [50]. Further, the developed charged double-layered interface was directly related to a capacitor ($C_{dl}$) in parallel with a resistor ($R_{dl}$). Both together were represented by a Constant Phase Element (CPE) with an empirical parameter 'n' ($0 \le n \le 1$) to represent the cell component, as shown in **Fig. 4(d)** [50]. If n = 1, the fabricated cell-device was considered to be an ideal capacitor; and if n = 0, then the fabricated cell-device was observed to be an ideal resistor and the impedance of CPE ($Z_{CPE}$) was calculated by equation 1.

$$Z_{CPE} = \frac{1}{(j\omega)^n \bullet Q_p} \quad (1)$$

The equivalent electrical circuit model of the fabricated device ($Z_{Fabricated\ device}$) was represented by equation 2:

$$Z_{\text{Fabricated device}}(\omega) = \left[R_s + \left(X_{C_p} \,||\, R_p\right)\right] \quad (2)$$

where, the $Z_{cell\ component}$ could be represented as in equation 3

$$Z_{cell\ component}(\omega) = \left[R_m \| C_m\right] \quad (3)$$

Hence, $Z_{cell\ component}$ was replaced in $Z_{Fabricated\ device}$ to derive $Z_{cell-device}$ in equation 4

$$Z_{\text{cell-device}}(\omega) = \left[R_s + \left(\left[R_m \| C_m\right] \| R_p\right)\right] \quad (4)$$

To represent the charged double-layered interface developed due to biological medium, the equation 4 was replaced with $Z_{CPE}$

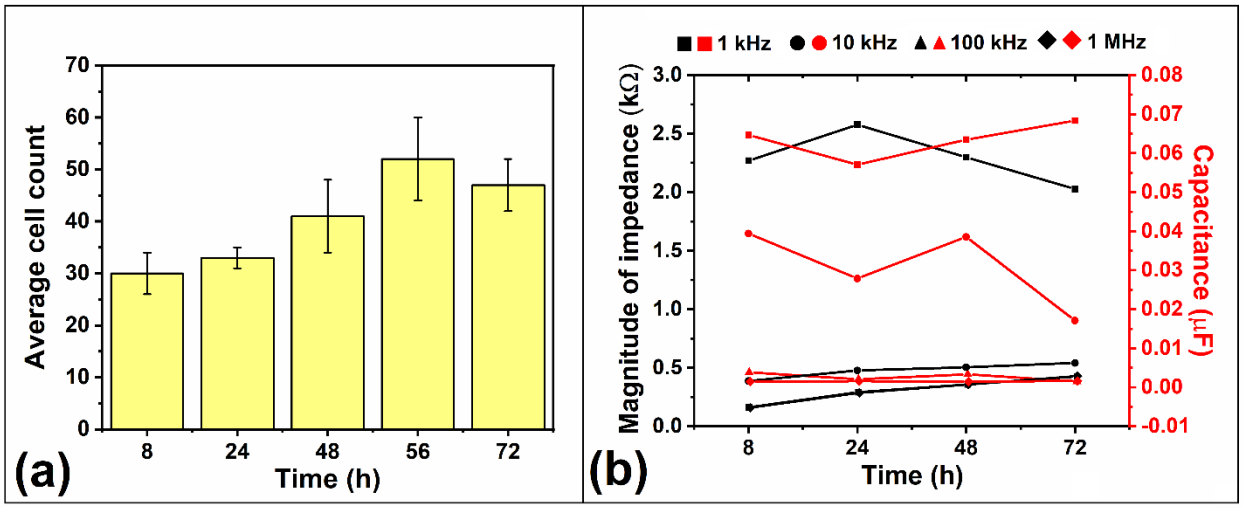


Fig. 5. (a) Average cell count at different time point, (b) Magnitude of impedance and Capacitance *vs.* time plot.

$$Z_{\text{cell-device}}(\omega) = \left[ R_s + \left( Z_{CPE_t} \middle|\middle| R_p \right) \right] \quad (5)$$

Simplifying equation 5, we got $Z_{cell-device}$

$$Z_{\text{cell-device}}(\omega) = \frac{R_s + R_p}{1 + (j\omega)^n Q_p \bullet R_p} \quad (6)$$

**Fig. 4(a)** shows device components/parameters, which was used to represent the fabricated device structure (ITO/$Al_2O_3$/ITO) in order to fit the fabricated device model using equation 2. **Fig. 4(b)** shows cell components/parameters and**Fig. 4(c)** shows fabricated device with cell components/parameters, which was modified as **Fig. 4(d)**, to represent the cell-device structure (ITO/cell-$Al_2O_3$/ITO) and equation 6 was used to fit this cell-device model. Further, the measured impedance data were fitted using a non-linear least mean curve fitting (NLLMCF) method [1], [54] to analyze the change in the progression of cellular functional behavior.

The EEC model parameters extracted in our study was given in **Table 1**. The result revealed that the resistance ($R_s$) and the reactance ($Q_p$) of $Z_{CPE}$ cell component got noticeably increased with a corresponding decrease in resistance ($R_p$) and empirical parameter (n). From NLLMCF, it is clear that the number of the biological cells present on the surface modulated the model parameters followed by the dynamic behaviour of the biological system. Further, to visualize frequency-dominated change over time, we studied the cell count and characteristic impedance change of the device. The average cell count and magnitude of impedance values and capacitance *vs.* time plot are represented in **Fig. 5**. The frequency-dependent changes were observed over time in terms of the magnitude of impedance and capacitance values with the progression of cellular growth. The outcomes revealed that the change in the characteristic electrical properties of the $Al_2O_3$ device was highly influenced by the progression of cellular processes, most likely due to the high dielectric constant. The transparent nature and air-stability of $Al_2O_3$ allowed us to visualize the changes in cellular morphology under an inverted microscope as well as facilitate continuous monitoring of cellular behaviour through analysing change in the electrical parameters.

## IV. Conclusion

In the present work, we have investigated the influence of myoblast progression in changing the characteristic electrical properties of the gelatin coated $Al_2O_3$ based device. The electrical properties varied with respect to every cellular function, such as cell adhesion, spreading, and proliferation. The effect induced by cellular functional behaviour was well correlated with both changes in the characteristic electrical property and microscopic observation of the cells as well as with an equivalent electrical model used. Hence, the fabricated device can be used for various bio-sensing applications wherein dynamic changes of the biological cells play a vital role.

## Acknowledgment

U. K. extends the acknowledgment for MHRD, India for the Institute Doctoral Research fellowship.

## References

[1] D. Das, G. S. Member, F. A. Kamil, S. Agrawal, K. Biswas, and S. Das, "Fragmental Frequency Analysis Method to Estimate Electrical Cell Parameters from Bioimpedance Study," vol. 63, no. 8, pp. 1991–2000, 2014.

[2] S. AlFadhli, "Missense Mutation in Cancer in Correlation to Its Phenotype – VHL as a Model," in *Mutations in Human Genetic Disease*, InTech, 2012.

[3] G. Yang *et al.*, "Dominant effects of an Msh6 missense mutation on DNA repair and cancer susceptibility," *Cancer Cell*, 2004, doi: 10.1016/j.ccr.2004.06.024.

[4] D. Sticker *et al.*, "Zirconium dioxide nanolayer passivated impedimetric sensors for cell-based assays," *Sensors Actuators, B Chem.*, 2015, doi: 10.1016/j.snb.2015.02.018.

[5] T. B. Tran, C. Baek, and J. Min, "Electric Cell-Substrate Impedance Sensing ( ECIS ) with Microelectrode Arrays for Investigation of Cancer Cell – Fibroblasts Interaction," pp. 1–12, 2016, doi: 10.1371/journal.pone.0153813.

[6] D. Mondal, R. Bose, and C. R. Chaudhuri, "Real-time monitoring of wound healing on nano-patterned substrates: Non-invasive impedance spectroscopy technique," *IEEE Transactions on Nanotechnology*. 2016, doi: 10.1109/TNANO.2016.2581212.

[7] Q. Liu, C. Wu, H. Cai, N. Hu, J. Zhou, and P. Wang, "Cell-Based Biosensors and Their Application in Biomedicine," 2014.

[8] A. D. Bendrea, L. Cianga, and I. Cianga, "Review paper: Progress in the field of conducting polymers for tissue engineering applications," *Journal of Biomaterials Applications*. 2011, doi: 10.1177/0885328211402704.

[9] S. P. Lin, S. Y. Huang, S. F. Chen, L. U. Vinzons, J. Y. Ciou, and P. J. Wong, "Investigation of the interfacial effects of small chemical-modified TiO2 NANOTUBES on 3T3 fibroblast responses," *ACS Appl. Mater. Interfaces*, 2014, doi: 10.1021/am503323y.

[10] N. J. Sniadecki, R. A. Desai, S. A. Ruiz, and C. S. Chen, "Nanotechnology for cell-substrate interactions," *Ann. Biomed. Eng.*, 2006, doi: 10.1007/s10439-005-9006-3.

[11] K. Kulangara and K. W. Leong, "Substrate topography shapes cell function," *Soft Matter*, 2009, doi: 10.1039/b910132m.

[12] S. H. Ku, J. Ryu, S. K. Hong, H. Lee, and C. B. Park, "General functionalization route for cell adhesion on non-wetting surfaces," *Biomaterials*, vol. 31, no. 9, pp. 2535–2541, 2010, doi: 10.1016/j.biomaterials.2009.12.020.

[13] R. Carbone *et al.*, "Biocompatibility of cluster-assembled nanostructured TiO2 with primary and cancer cells," *Biomaterials*, vol. 27, no. 17, pp. 3221–3229, 2006, doi: 10.1016/j.biomaterials.2006.01.056.

[14] M. Ermis, E. Antmen, and V. Hasirci, "Micro and Nanofabrication methods to control cell-substrate interactions and cell behavior: A review from the tissue engineering perspective," *Bioactive Materials*, vol. 3, no. 3. KeAi Communications Co., pp. 355–369, Sep. 01, 2018, doi: 10.1016/j.bioactmat.2018.05.005.

[15] A. Dolatshahi-Pirouz, M. Nikkhah, K. Kolind, M. R. Dokmeci, and A. Khademhosseini, "Micro- and Nanoengineering Approaches to Control Stem Cell-Biomaterial Interactions," *J. Funct. Biomater.*, 2011, doi: 10.3390/jfb2030088.

[16] C. Bettinger, R. Langer, and J. Borenstein, "Engineering substrate micro- and nanotopography to control cell function," *Angew. Chem. Int. Ed. Engl.*, 2009, doi: 10.1002/anie.200805179.

[17] D. Mondal and C. Roy Chaudhuri, "Real time in vitro monitoring and impedance modeling of mammalian cell activities on planar ECIS and micro/nano patterned cytosensors," *ISSS J. Micro Smart Syst.*, 2018, doi: 10.1007/s41683-018-0024-4.

[18] A. Andrzejewska *et al.*, "Labeling of human mesenchymal stem cells with different classes of vital stains: Robustness and toxicity," *Stem Cell Res. Ther.*, 2019, doi: 10.1186/s13287-019-1296-8.

[19] X. W. Hua, Y. W. Bao, Z. Chen, and F. G. Wu, "Carbon quantum dots with intrinsic mitochondrial targeting ability for mitochondria-based theranostics," *Nanoscale*, 2017, doi: 10.1039/c7nr03658b.

[20] H. J. Yoon *et al.*, "Sensitive capture of circulating tumour cells by functionalized graphene oxide nanosheets," *Nat. Nanotechnol.*, 2013, doi: 10.1038/nnano.2013.194.

[21] S. Prendecka, J. Frankowski, G. Sobieszek, L. Kapka-Skrzypczak, A. Skwarek-Dziekanowska, and T. Maleckaa-Masalska, "Electric Cell Substrate Impedance Sensing (ECIS) as a unique technique in cancer metastasis research," *J. Pre-Clinical Clin. Res.*, vol. 12, no. 4, 2018.

[22] M. Amini, J. Hisdal, and H. Kalvøy, "Applications of bioimpedance measurement techniques in tissue engineering," *J. Electr. Bioimpedance*, vol. 9, no. 1, 2018.

[23] U. Kasiviswanathan, S. Poddar, C. Kumar, S. Jit, S. K. Mahto, and N. Sharma, "A portable standalone wireless electric cell-substrate impedance sensing (ECIS) system for assessing dynamic behavior of mammalian cells," *J. Anal. Sci. Technol.*, vol. 11, no. 1, p. 25, 2020, doi: 10.1186/s40543-020-00223-9.

[24] S. E. De León, A. Pupovac, and S. L. McArthur, "Three-Dimensional (3D) cell culture monitoring: Opportunities and challenges for impedance spectroscopy," *Biotechnology and Bioengineering*. 2020, doi: 10.1002/bit.27270.

[25] S. H. Jeong, D. W. Lee, S. Kim, J. Kim, and B. Ku, "A study of electrochemical biosensor for analysis of three-dimensional (3D) cell culture," *Biosens. Bioelectron.*, 2012, doi: 10.1016/j.bios.2012.02.039.

[26] P. Daza, A. Olmo, D. Canete, and A. Yúfera, "Monitoring living cell assays with bio-impedance sensors," *Sensors Actuators, B Chem.*, 2013, doi: 10.1016/j.snb.2012.09.083.

[27] A. Susloparova, D. Koppenhöfer, J. K. Y. Law, X. T. Vu, and S. Ingebrandt, "Electrical cell-substrate impedance sensing with field-effect transistors is able to unravel cellular adhesion and detachment processes on a single cell level," *Lab Chip*, 2015, doi: 10.1039/c4lc00593g.

[28] F. Asphahani and M. Zhang, "Cellular impedance biosensors for drug screening and toxin detection," *Analyst*. 2007, doi: 10.1039/b704513a.

[29] C. J. Flaim, S. Chien, and S. N. Bhatia, "An extracellular matrix microarray for probing cellular differentiation," *Nat. Methods*, 2005, doi: 10.1038/nmeth736.

[30] I. Park *et al.*, "Electrical impedance monitoring of C2C12 myoblast differentiation on an indium tin oxide electrode," *Sensors*, vol. 16, no. 12, p. 2068, 2016.

[31] J. A. Stolwijk and J. Wegener, "Impedance-Based Assays Along the Life Span of Adherent Mammalian Cells In Vitro: From Initial Adhesion to Cell Death," *Label-Free Monit. Cells Vitr.*, pp. 1–75, 2019.

[32] J. L. Hammond, N. Formisano, P. Estrela, S. Carrara, and J. Tkac, "Electrochemical biosensors and nanobiosensors," *Essays Biochem.*, 2016, doi: 10.1042/EBC20150008.

[33] T. Schmiedinger *et al.*, "Interdigitated aluminium and titanium sensors for assessing epithelial barrier functionality by electric cell-substrate impedance spectroscopy (ECIS)," *Biomed. Microdevices*, 2020, doi: 10.1007/s10544-020-00486-4.

[34] L. Zhang *et al.*, "Plasmonic Al nanopyramid array sensor for monitoring the attaching and spreading of cells," *Sensors Actuators, B Chem.*, 2019, doi: 10.1016/j.snb.2018.10.023.

[35] F. A. Banville *et al.*, "Nanoplasmonics-enhanced label-free imaging of endothelial cell monolayer integrity," *Biosens. Bioelectron.*, 2019, doi: 10.1016/j.bios.2019.111478.

[36] U. Kasiviswanathan, C. Kumar, S. Poddar, S. Jit, S. K. Mahto, and N. Sharma, "Fabrication of MSM Based Biosensing Device for Assessing Dynamic Behavior of Adherent Mammalian Cells," *IEEE Sens. J.*, vol. 20, no. 17, pp. 9652–9659, 2020, doi: 10.1109/JSEN.2020.2990919.

[37] W. Li, B. Kabius, and O. Auciello, "Science and technology of biocompatible thin films for implantable biomedical devices," in *2010 Annual International Conference of the IEEE Engineering in Medicine and Biology Society, EMBC'10*, 2010, doi: 10.1109/IEMBS.2010.5628056.

[38] D. S. Finch, T. Oreskovic, K. Ramadurai, C. F. Herrmann, S. M. George, and R. L. Mahajan, "Biocompatibility of atomic layer-deposited alumina thin films," *J. Biomed. Mater. Res. - Part A*, 2008, doi: 10.1002/jbm.a.31732.

[39] J. Y. Tsao *et al.*, "Ultrawide-Bandgap Semiconductors: Research Opportunities and Challenges," *Advanced Electronic Materials*. 2018, doi: 10.1002/aelm.201600501.

[40] S. Riaz, Sajid-ur-Rehman, M. Abutalib, and S. Naseem, "Structural, Optical, and Dielectric Properties of Aluminum Oxide Nanofibers Synthesized by a Lower-Temperature Sol–Gel Approach," *J. Electron. Mater.*, 2016, doi: 10.1007/s11664-016-4754-4.

[41] S. Shi, S. Qian, X. Hou, J. Mu, J. He, and X. Chou, "Structural and optical properties of amorphous Al2O3 thin film deposited by atomic layer deposition," *Adv. Condens. Matter Phys.*, 2018, doi: 10.1155/2018/7598978.

[42] S. Rajiv *et al.*, "Comparative cytotoxicity and genotoxicity of cobalt (II, III) oxide, iron (III) oxide, silicon dioxide, and aluminum oxide nanoparticles on human lymphocytes in vitro," *Hum. Exp. Toxicol.*, 2016, doi: 10.1177/0960327115579208.

[43] Z. X. Qiang, Y. L. Hong, A. Tang meng, and P. Y. Pu, "ZnO, TiO2, SiO2, and Al2O3 Nanoparticlesinduced Toxic Effects on Human Fetal Lung Fibroblasts," *Biomed Env. Sci,* 2011, doi: 10.3967/0895.

[44] U. Kasiviswanathan, C. Kumar, S. Poddar, S. Jit, N. Sharma, and S. K. Mahto, "Functional Behaviour of the Primary Cortical Neuronal Cells on the Large Surface of TiO2 and SnO2 based Biosensing Device," *IEEE Trans. Nanobioscience*, p. 1, 2021, doi: 10.1109/TNB.2021.3058332.

[45] G. Rawat, D. Somvanshi, H. Kumar, Y. Kumar, C. Kumar, and S. Jit, "Ultraviolet Detection Properties of p-Si/n-TiO2 Heterojunction Photodiodes Grown by Electron-Beam Evaporation and Sol-Gel Methods: A Comparative Study," *IEEE Trans. Nanotechnol.*, 2016, doi: 10.1109/TNANO.2015.2512565.

[46] S. Ratan, C. Kumar, A. Kumar, D. K. Jarwal, and A. K. Mishra, "Fabrication and Characterization of Titanium Dioxide Based Pd / TiO 2 / Si MOS Sensor for Hydrogen Gas," vol. 18, no. 10, pp. 3952–3959, 2018.

[47] H. Kumar *et al.*, "Kink effect in TiO 2 embedded ZnO quantum dot-based thin film transistors," vol. 53, no. 4, pp. 15–16, 2017, doi: 10.1049/el.2016.3595.

[48] K. S. Shamala, L. C. S. Murthy, and K. N. Rao, "Studies on optical and dielectric properties of Al2O 3 thin films prepared by electron beam evaporation and spray pyrolysis method," *Mater. Sci. Eng. B Solid-State Mater. Adv. Technol.*, 2004, doi: 10.1016/j.mseb.2003.09.036.

[49] C. K. Balavigneswaran *et al.*, "Tailored Chemical Properties of 4-Arm Star Shaped Poly(d, l -lactide) as Cell Adhesive Three-Dimensional Scaffolds," *Bioconjug. Chem.*, 2017, doi: 10.1021/acs.bioconjchem.7b00071.

[50] G. Kumar, U. Kasiviswanathan, S. Mukherjee, S. K. Mahto, N. Sharma, and R. Patnaik, "Changes in electrolyte concentrations alter the impedance during ischemia-reperfusion injury in rat brain," *Physiol. Meas.*, Sep. 2019, doi: 10.1088/1361-6579/ab47ee.

[51] A. R. A. Rahman, J. Register, G. Vuppala, and S. Bhansali, "Cell culture monitoring by impedance mapping using a multielectrode scanning impedance spectroscopy system (CellMap)," *Physiol. Meas.*, 2008, doi: 10.1088/0967-3334/29/6/S20.

[52] T. Gerasimenko *et al.*, "Impedance Spectroscopy as a Tool for Monitoring Performance in 3D Models of Epithelial Tissues," *Frontiers in Bioengineering and Biotechnology*. 2020, doi: 10.3389/fbioe.2019.00474.

[53] B. Maundy and A. S. Elwakil, "Extracting single dispersion Cole-Cole impedance model parameters using an integrator setup," *Analog Integr. Circuits Signal Process.*, 2012, doi: 10.1007/s10470-011-9751-1.

[54] G. Kemmer and S. Keller, "Nonlinear least-squares data fitting in Excel spreadsheets," *Nat. Protoc.*, 2010, doi: 10.1038/nprot.2009.182.